Physio-geometrical Characterization of Combustion Generated Nano-particle Emissions from a Palm Oil Based Biodiesel Fueled Agricultural Engine

Monthiean Rattanathom, Sathaporn Chuepeng* and Suabsakul Gururatana

Abstract

A physio-geometry of the particulate matter emitted from the combustion chamber becomes growingly important as it can affect to the exhaust gas after-treatment devices. The surface area of the particles will play a vital role as it is a site for catalytic combustion to be taken place. This work investigates the combustion characteristics and particulate matter related emissions of a single-cylinder agricultural diesel engine fueled with palm oil based biodiesel at constant speed and loads. The experimental results from the combustion analysis using an indicating system reveal that the biodiesel initiates the combustion faster with pronounce premixed combustion regime than that of diesel fuel. The specific fuel consumption of biodiesel was greater that leads to a slight reduction in brake thermal efficiency compared with diesel. Biodiesel combustion reduces smoke opacity that is ultimately in-line with the total particle mass. The nano-particle emissions was characterized by an electrical mobility spectrometer and analyzed in terms of number, surface area, and mass. The particle number size distribution was found to be in the nucleation and accumulation modes, and the total particle number increased with smaller size when fueling with biodiesel. The distributions of the particle surface area and mass are left-screwed in the log-scale of area and mass diameter ranges, respectively, leading to the lesser total particle areas and masses for biodiesel fuel at smaller size.

Keywords : Biodiesel, Combustion, Diesel, Distribution, Emission, Engine, Particulate matter

---

Automotive Technology and Alternative Energy Research Group, Department of Mechanical Engineering, Faculty of Engineering at Sriracha, Kasetsart University Sriracha Campus, 199 Sukhumvit Road, Chonburi 20230, Thailand.

* Corresponding author, E-mail: schuepeng@eng.src.ku.ac.th Received 7 September 2017, Accepted 23 November 2017

Nomenclature

a	Area concentration
A	Total area concentration
AMD	Area mean diameter
bsfc	Brake specific fuel consumption
CMD	Count mean diameter
DAQ	Data acquisition
DBE	Diesel-biodiesel-ethanol blends
D_p	Equivalent diameter
$dQ_n/d\theta$	Heat release rate
EGR	Exhaust gas recirculation
EMS	Electrical mobility spectrometer
FAME	Fatty acid methyl ester
IMEP	Indicated mean effective pressure
l	Minimum particle size
m	Mass concentration
M	Total mass concentration
$\dot{m}_f$	Fuel mass consumption rate
MMD	Mass mean diameter
n	Number concentration
N	Total number concentration
N	Engine speed
p	In-cylinder pressure
P_b	Brake power
P_i	Indicated power
PM	Particulate matter
Q_{HV}	Lower heating value
rpm	Revolution per minute
TEM	Transmission electron microscopy
TGA	Thermogravimetric analysis
T_i	Indicated torque
u	Maximum particle size
V	Cylinder volume
V_d	Displaced volume
$W_{c,i}$	Indicated work per cycle
γ	Specific heat ratio
η_{th}	Brake thermal efficiency
θ	Crank angle
ρ	Density of particulate matter

1. Introduction

Biodiesel nowadays is one of the promising alternative fuels for road transportation as its properties are comparable to fossil diesel fuel [1] that can be partially substituted to diesel for fueling diesel vehicles in many countries. Biodiesel can be produced from numerous feedstock such as rapeseed [2], jatropha [3-4], palm oil [5], waste cooking oils [6-8], castor oil [9], soybean [10], and karanja [11] by various techniques. Apart from bi-mixture, biodiesel has been mixed as tri-fuels with other amalgamable compositions such as Fischer-Tropsch synthetic diesel fuel [12], oxygenated hydrocarbons [13], ethanol [14], and pentanol [15] in order to improve engine performance and combustion generated exhaust emissions.

In aspect of environment, many methods for mitigating diesel exhaust toxics have been developed. Hedayat *et al.* (2016) [16] found out the particulate oxidative potentiality of biodiesel with various oxygenated compounds. Shukla *et al.* (2017) [17]

applied non-noble metal based biodiesel oxidation catalyst for improving particle number emission of biodiesel exhaust. Karavalakis *et al*. (2017) [18] indicated the impacts of biodiesel on redox and proinflammatory properties of particulate matter. Martin *et al*. (2017) [19] pointed out the biodiesel effects on non-road heavy duty diesel engine particulate matter emissions, composition and cytotoxicity.

In terms of engine performance, Wang *et al*. (2013) [20] compared combustion characteristics and brake thermal efficiency of a heavy-duty diesel engine fueled with diesel and biodiesel at high altitude. The investigation revealed some results that were in agreement with those at ground level. Biodiesel fueled engine consumed more fuel and produced less brake thermal efficiency than those of diesel fueled engine. Tse *et al*. (2015) [21] investigated on combustion characteristics and particle emission from a diesel engine fueled with diesel-biodiesel-ethanol blends (DBE). The DBE can better reduce particulate matter than biodiesel and diesel but nitrogen oxides increased.

A close consideration into diesel particulate matter has revealed several key findings. The typical particle size characterization of diesel particulate matter is in form of tri-modal and lognormal distribution [22]. The nucleation mode includes light-weight spherical primary particles ranging from 5 to 50 nm diameter. Subsequently, the accumulation mode, primary particles are agglomerated into aggregates, fractal-like particles having equivalent diameter ranging from 50 to 1,000 nm with a lower number of particles but higher total particle mass compared to the nucleation mode. Third, the coarse mode contains particles larger than 1,000 nm in equivalent diameter.

A number of published work versatilely studied on particulate matter (PM) from the combustion of neat or blended biodiesel fuels. At low temperature combustion, Jung *et al*. (2016) [23] assessed the PM in exhaust gas of biodiesel using thermogravimetric analysis (TGA), elemental analysis, and transmission electron microscopy (TEM). Thitipatanapong *et al*. (2015) [24] also used the TGA in characterizing PM component from the combustion of palm-oil based biodiesel blended with fossil diesel in the volumetric diesel:biodiesel proportion of 95:5, commonly called B5. Rahman *et al*. (2014) [25] found out that the different physical properties and chemical composition of biodiesel affect to the PM. The outcomes are in-line with work accomplished by Pinzi *et al*. (2013) [26] that varied biodiesel fatty acid composition. Rounce *et al*. (2012) [27] speciated hydrocarbon emissions, analyzed the mass reduction through TGA, and studied the number-size distribution of the PM from biodiesel combustion.

Morphologically, Savic *et al*. (2016) [28] explored the influence of biodiesel fuel composition on microstructure of particles emitted from diesel engines. Meanwhile, Salamanca *et al*. (2012) [29] indicated the influence of palm oil biodiesel on the chemical and

morphological characteristics of particulate matter emitted by a diesel engine. Physical properties and morphology become more important than other aspects as they may affect to particulate filter behavior of a diesel engine fueled with biodiesel [30]. By this scenario, there are some knowledge gaps of PM characterization, especially for palm oil based biodiesel that could affect to exhaust gas after-treatment devices.

This research work aims to study the combustion characteristics, fuel consumption and efficiency, and PM related emissions from the combustion of palm oil based biodiesel. The experimental will be conducted using an agricultural single cylinder diesel engine running at a constant speed, low and medium loads. Smoke opacity, particle number-, surface area-, and mass- size distributions with their corresponding total number-, area-, and mass- concentrations will be analyzed and discussed.

2. Materials and method

2.1 Engine test bench

The experimental study was conducted using an agricultural diesel engine (Kubota, Model RT 100 DI PLUS ES) on the test bench equipped with measurement apparatus as shown in Fig. 1. The fuel injection system of the test engine was a mechanical pump-line-nozzle type. The specification is concisely shown in Table 1.

The engine was loaded by a pony brake engine dynamometer with the maximum capacity of 15 kW. A load cell for the engine dynamometer was from Vishay Tedea-Huntleigh model 613 standing with the maximum capacity of 50 kg load. Its sensitivity is 2 mV/V and its total error is ± 0.02 % of rated output. The measurement accuracy for revolution speed from the engine dynamometer in speed control mode was ± 10 rpm. The diagram of the engine test rig is depicted in Fig. 1.

Table 1 Engine specification

Properties	Specification
Engine type	1-cylinder, water cooled
Combustion type	Direct injection
Bore x Stroke	88 mm × 90 mm
Displaced volume	547 cc
Maximum power	7.4 kW at 2,400 rpm
Maximum torque	33.4 Nm at 1,600 rpm
Compression ratio	18:1

The experimental system also involved other standard engine test rig instrumentation, i.e. several local temperature measurement devices. Recording of atmospheric conditions in terms of temperature, pressure, and humidity was accomplished in order to use as input to the software for cylinder pressure corrections. All these data were recorded by a data acquisition board (National Instruments, Model USB-6218) installed in a Windows-based PC with the in-house developed LabVIEW based software.

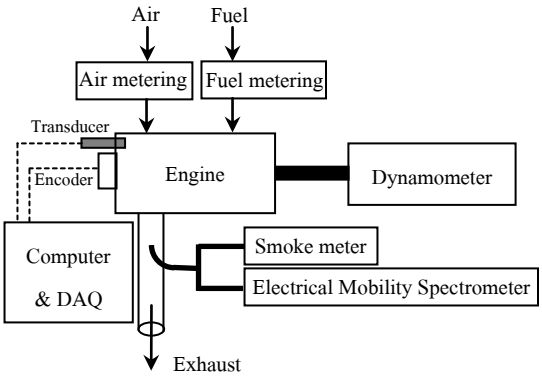

Fig. 1. Schematic diagram of engine test rig

2.2 Air and fuel measurement units

The air flow into the engine is measured by a Testo model 435 flow measurement unit with accuracy in the range of ± 0.3% of reading. Diesel fuel flow rate was measured on mass basis using a balance from CST model CDR-3 with accuracy of ± 0.05 g. The fuel temperature was control at 40±1°C using a liquid-to-liquid heat exchanger immersed in a bath Lauda model Ecoline 011 with temperature controller from Lauda model E200.

2.3 Engine indicating system

Cylinder pressure data corresponding to the position of the crankshaft was used to study the combustion characteristics. The combustion pressure in the cylinder was measured by a pressure transducer (Kistler, Model 6052C) with its sensitivity of -19.90 pC/bar at 200°C and linearity of ± 0.4% FSO. The signal has been sent to the charge amplifier (Dewetron, Model DEWE-30-4) in order to magnify and filter the signal from the pressure transducer. Meanwhile, the incremental shaft encoder (Baumer Electric, Model BDK 16.05A360-5-4) was used to determine the position of the engine crankshaft rotation. The sampling rate of position measurement of the shaft was set to 360 pulses per revolution.

Table 2 Fuel properties

Analysis	Method	Diesel	Biodiesel
Flash point (°C)	ASTM D93-11	60.0	131.0
Density at 15°C (kg/l)	ASTM D4052-11	0.8255	0.8752
Kinematic viscosity at 40°C (cSt)	ASTM D445-11a	2.9	4.5
Sulfur content (%wt)	ASTM D2622-10	0.0037	0.0002
Cetane number	EN 14078-03	58.8	62.4
Lower heating value (MJ/kg)	ASTM D4809-13	42.8	37.3

All signals are sent to the data acquisition system (Dewetron, Model DEWE-ORION-0816-100x) at the sampling rate of 1 MS/s. The cylinder pressure traces were analyzed using the DEWEsoft V6.6.9 software. Cylinder pressure traces of 100 consecutive cycles were averaged as statistical values and were then used to represent the values of the combustion characteristics in each test condition.

2.4 Fuel

There were two types of fuel used in the test: diesel and biodiesel. The diesel fuel contains a trace of fatty acid methyl ester (FAME) by local regulation (volumetric blend of 95% petroleum diesel and 5% palm-based biodiesel). Meanwhile, the neat biodiesel was palm- based. Some of their key properties are numerated in Table 2.

2.5 Particulate matter and smoke determination

Smoke was measured using a Motorscan Smoke Module 9010 based on the light intensity absorbed and smoke will be reported in term of opacity percentage. The measurement range is 0 to 100 % opacity and the accuracy is ±0.1 % opacity.

The measurement of particle number size distribution was a full-flow sampling of a small portion of the exhaust gas, approximately 40 cm downstream of the exhaust manifold. The PM contained exhaust gas was isokinetically drawn at the constant volumetric flow rate of 3 lpm into an Electrical Mobility Spectrometer (EMS) (Fabix, Model DusTEC). The EMS is able to measure particles in the size range of 10 to 2,200 nm at 60 s time response [31]. The particle number size distributions shown in the following sections are one minute averages that are representatives for each steady state engine test condition.

The distribution of particle number concentration is presented in the unit of number per cubic meter, over the interval of particle size in the logarithmic scale. The particle size is shown as an equivalent diameter (D_p) of count, area, or mass mean diameters as the particle is not apparently spherical.

Table 3 Test conditions

Condition	Speed (rpm)	Load (bar IMEP)
1	1,700	3.3
2	1,700	6.6

2.6 Test condition

The engine was tested under the operating condition as shown in Table 3 without exhaust gas recirculation (EGR) and without engine modification. The speed chosen is by the frequently use of loaded application (agricultural purposes) and is near by the maximum torque occurrence produced by the engine. Furthermore, the constant engine loads of 3.3 and 6.6 bar IMEP values were respectively tested as to simulate for 25% and 50% of the maximum engine load, regularly used in real engine operating conditions.

2.7 Definition of parameters

Indicated work per cycle ($W_{c,i}$) is the work transferred from gas inside the cylinder to the piston, following [32]:

$$W_{c,i} = \oint p dV \quad (1)$$

where p is in-cylinder pressure and V is cylinder volume.

Indicated work per cycle ($W_{c,i}$), indicated power (P_i) and indicated torque (T_i) are related with engine speed (N) by the equation

$$P_i = \frac{W_{c,i}N}{2} \quad (2)$$

and

$$P_i = 2\pi NT_i \quad (3)$$

Indicated mean effective pressure (IMEP) is the value of pressure indicating the performance of an engine. The IMEP value is used to compare performance of two engines having different displaced volume (V_d), obtained from

$$IMEP = \frac{2P_i}{V_d N} \quad (4)$$

The brake specific fuel consumption (bsfc) is the fraction between fuel mass consumption rate ($\dot{m}_f$) and brake power (P_b), obtained from

$$bsfc = \frac{\dot{m}_f}{P_b} \quad (5)$$

The brake thermal efficiency (η_{th}) is the ratio between produced work per cycle and chemical energy in the fuel, calculated from

$$\eta_{th} = \frac{P_b}{\dot{m}_f Q_{HV}} \quad (6)$$

where Q_{HV} is the fuel lower heating value and P_b is brake power.

The values of in-cylinder pressure corresponding to crankshaft angle position are used to obtain the heat release rate ($dQ_n/d\theta$) of the engine. The heat release rate can be calculated by fuel chemical energy suppressed by the heat loss in to a coolant system. The calculation condition is assumed to be the ideal gas condition in angle position domain, following:

$$\frac{dQ_n}{d\theta} = \frac{\gamma}{\gamma\text{-}1} p \frac{dV}{d\theta} + \frac{1}{\gamma\text{-}1} V \frac{dp}{d\theta} \quad (7)$$

where θ is crank angle in degree and γ is specific heat ratio. The latter was directly obtained from each experimental condition assuming that the pV^{γ} was constant in the compression and expansion strokes.

The ignition delay is defined as the time interval in degree of the crankshaft from the start of injection of the diesel fuel to where the rate of heat release turns to the positive value, called the start of combustion. The latter occurs after the diesel fuel is injected and gets heat from surrounding to vaporize (negative value of the heat release rate). The combustion duration is defined as the time interval in degree of the crankshaft from the start of combustion to the end of combustion where the heat release rate turns into zero in the expansion stroke.

For the PM characterization, the number concentration (n) can be directly obtained by the measurement while the (surface) area and mass concentrations can be calculated by

Area:

$$a = \pi D_p^3 n \quad (8)$$

Mass:

$$m = \frac{\rho \pi D_p^3 n}{6} \quad (9)$$

where n, a and m are number, area and mass concentrations, respectively. D_p is equivalent diameter and ρ is density of the particulate matter. In fact, density is dependent on particle diameter and engine operating condition [22], while the particle density of 1.2 kg·m^{-3} was chosen for the purpose of comparison.

For the total concentrations of number, area, and mass (N, A, and M respectively), each quantity in all size ranges was summarized and can be calculated by:

Number:

$$N = \sum_{l}^{u} n \quad (10)$$

Area:

$$A = \sum_{l}^{u} a \quad (11)$$

Mass:

$$M = \sum_{l}^{u} m \quad (12)$$

where l and u are the minimum and maximum particle sizes, respectively.

The PM mean diameters can be calculated in three physical categories: count mean diameter (CMD), area mean diameter (AMD), and mass mean diameter (MMD) following these formulae.

Number:

$$CMD = \frac{\sum_{l}^{u} nD_p}{N} \quad (13)$$

Area:

$$AMD = \frac{\sum_{l}^{u} aD_p}{A} \quad (14)$$

Mass:

$$MMD = \frac{\sum_{l}^{u} mD_p}{M} \quad (15)$$

3. Results and discussion

In this section, combustion characteristics, fuel consumption and efficiency, and PM related emissions are compared and discussed.

3.1 Combustion characteristics

The analysis of combustion characteristics presented in the section includes the cylinder pressure traces, peak pressure, heat release rate, start of combustion, and combustion duration.

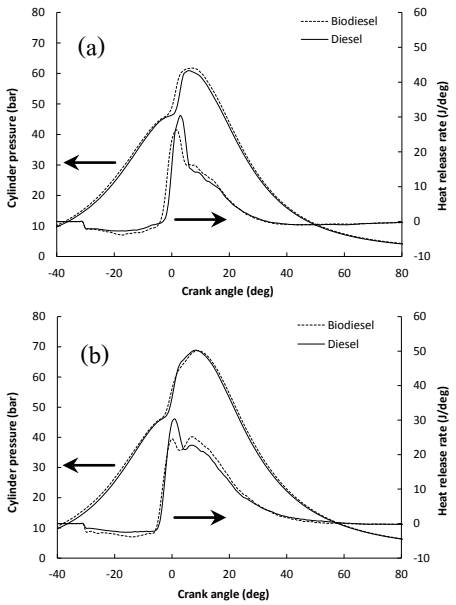

Fig. 2. In-cylinder pressure and heat release rate at 1,700 rpm (a) 3.3 bar IMEP and (b) 6.6 bar IMEP

Fig. 2 illustrates the traces of cylinder pressure and the rates of heat release versus crank angle over the late compression and the early expansion strokes of the engine running on biodiesel at 3.3 and 6.6 bar IMEP loads with those of diesel fuel for comparison.

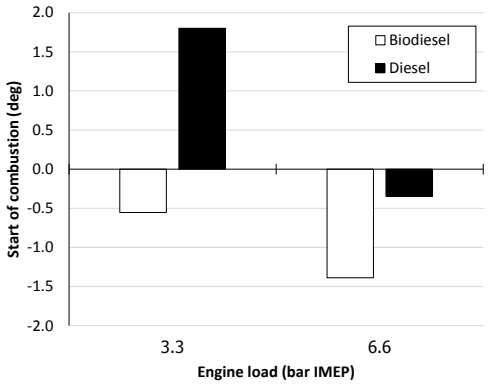

Fig. 3. The start of combustion for diesel and biodiesel

For the same load, the combustion of biodiesel apparently resulted in an increased rate of the fuel burning in the premixed phase, with the combustion advanced to earlier crank angle positions and peak pressure values increased over the diesel fuel combustion. These effects can also be seen for different engine loads. The negative heat release rates for both fuels obviously seen after the start of injection denotes the fuel that requires heat for vaporization prior to the combustion.

The starts of combustion for biodiesel combustion are shown in Fig. 3. It is apparently that the start of combustion for biodiesel was taken place earlier than that of diesel fuel combustion, by 2.36° and 1.04° crank angle at 3.3 and 6.6 bar IMEP loads, respectively. Regardless of fuel type used, the start of combustion was advanced when running the engine at higher load. Ignition delay can be represented by comparing the start of combustion that the obtained results indicate the shorter ignition delay of biodiesel than diesel fuel combustion.

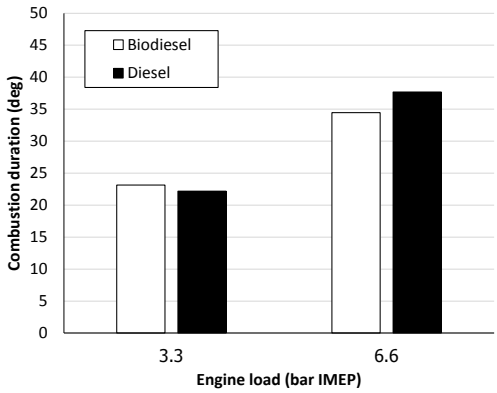

Fig. 4. Combustion duration

For other physical properties of biodiesel, the advanced injection timing and increased injection rate and pressure have been frequently reported for the use of biodiesel e.g. density, viscosity, and bulk modulus of compressibility. Due to the biodiesel's lower compressibility, the pressure in the pump-line-nozzle fuel injection system can be built up and distributed quicker even at the same pump timing, resulting in the advance of injection [33].

Fig. 4 illustrates the combustion duration for biodiesel and diesel fuel combustion at the two engine loads. At the higher load, the diesel fuel burned longer (~4° crank angle) than that of biodiesel while at the lower load, the difference in combustion duration was

insignificantly seen (0.98° crank angle). The biodiesel combustion was prone to be shorter in combustion duration (Fig. 4), due to the earlier start of combustion under the same engine load (Fig. 3) with the increased rate of the fuel burning in the premixed phase (Fig. 2). Regardless of the fuel type used at the higher load, the engine doses more fuel in to the combustion chamber [32]. This causes a longer time for fuel to burn in the combustion chamber, and hence longer combustion duration.

3.2 Fuel consumption and efficiency

The brake specific fuel consumption is shown in Fig. 5. Outwardly, the case of biodiesel consumed more fuel than the case of diesel fuel. The heating value of the biodiesel fuel is lower by approximately 13% (see Table 2 for comparison) compared to that of diesel fuel. Therefore, biodiesel requires a larger amount of fuel injected into the combustion chamber to produce the same power. This has caused the slight decrease in engine brake thermal efficiency (Fig. 6) compared to the case of diesel fuel by 6% and 12% at the engine loads of 3.3 and 6.6 bar IMEP, respectively.

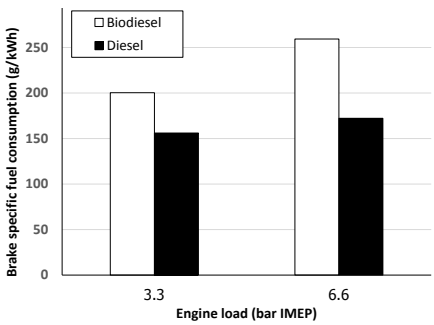

Fig. 5. Brake specific fuel consumption

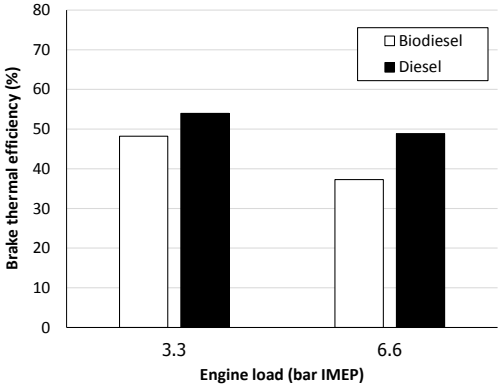

Fig. 6. Brake thermal efficiency

3.3 Particulate matter related emissions

The emissions related to particulate matter described in this section are associated to smoke opacity, particle number-, surface area-, and mass- size distributions with their corresponding total number-, area-, and mass- concentrations.

Fig. 7 shows smoke opacity from the combustion of biodiesel and diesel fuels at the two engine loads. For both loads, biodiesel combustion resulted in the lower level of smoke opacity than that from diesel fuel combustion. In the meantime, regardless of fuel type, the engine running at the higher load generated greater level of black smoke whereas the fuel was injected in greater amount within limited combustion time and oxidizer [33]. Apart from the oxygen content of the biodiesel that may contribute to improved fuel oxidation in locally rich in fuel combustion zones, resulting in the reduction of smoke. The reduction of smoke for biodiesel over diesel fuel can also be attributed to its significantly lower sulfur content in the

fuel (see Table 2 for comparison). By this key factor, sulfur compound has been recognized for being a part of a solid carbon contained core of the particulate matter [34].

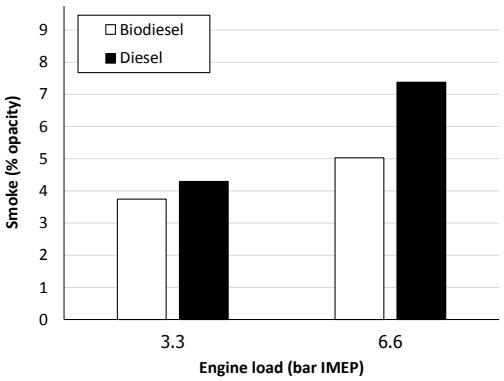

Fig. 7. The effects of engine load on smoke

Fig. 8 shows the distribution of particle number concentration over the range of count mean diameter (CMD) from biodiesel and diesel combustions at 3.3 and 6.6 bar IMEP loads, 1,700 rpm. At these loads, regardless of fuel type used, the distributions are tri-modal log-normal in the CMD range. Biodiesel particles show a greater concentration in the nucleation and accumulation modes for both loads while the diesel particles show a greater concentration in the coarse mode, particularly at the higher load. One of the main parameters related to the increased concentration of particles at small sizes is the increase in fuel injection pressure for biodiesel. In a pump-line-nozzle fuel injection system, the increased injection pressure of biodiesel was due to its higher density and viscosity and bulk modulus of compressibility [37]. This yields better fuel atomization by increasing the number and shifting the fuel droplets to smaller sizes.

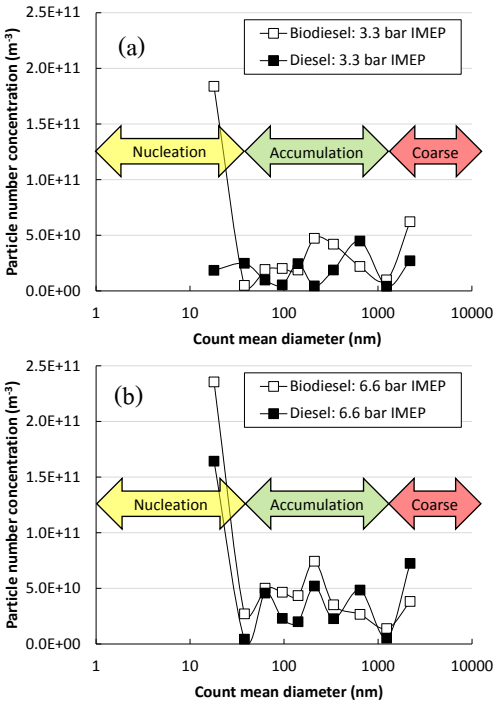

Fig. 8 Particle number size distribution for the engine at (a) 3.3 bar IMEP and (b) 6.6 bar IMEP loads

Fig. 9 shows the plots of the total particle number calculated using Eq. (10) and the corresponding CMD. The total particle numbers have shown to be higher for biodiesel at smaller size for the two load conditions tested. The total particle numbers for biodiesel and diesel fuels were in the ranges of 4.3×10^{11} to 5.0×10^{11} m^{-3} and 1.8×10^{11} to 4.6×10^{11} m^{-3}, respectively. The count mean diameter for biodiesel and diesel fuels were in the ranges of 279 to 457 nm and 495 to 586 nm, respectively. Furthermore, the engine running on the higher load generated higher amount of total particle number at smaller size. The engine running at

the higher load injected a greater fuel amount that was prone to emit the particles at higher amount and smaller size [36]. However, the total particle number concentration can also reduce corresponding to the enlarged particle size during high engine load as higher degree of coagulation of nanoparticles occurs [35].

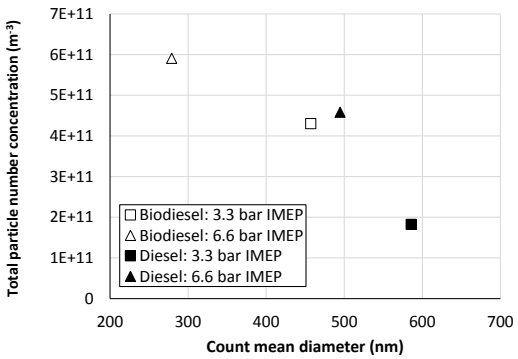

Fig. 9 Relationship between total particle number and count mean diameter

One of the main reasons for the higher total particle number for biodiesel combustion is oxygen content in the fuel. This yields better fuel atomization with oxidizer among bulk of the injected fuel by increasing the number and shifting the fuel droplets to smaller sizes. The above trends of particles are similar to the results obtained by Chuepeng *et al*. (2008) [35], while contrary to the work done by Chuepeng *et al*. (2009) [36] where the exhaust gas recirculation was in use. In fact, larger aggregates can be formed when the particle number is higher [37]. However, the combustion at this load in the agricultural engine did not reach the stage that the larger aggregates to be formed.

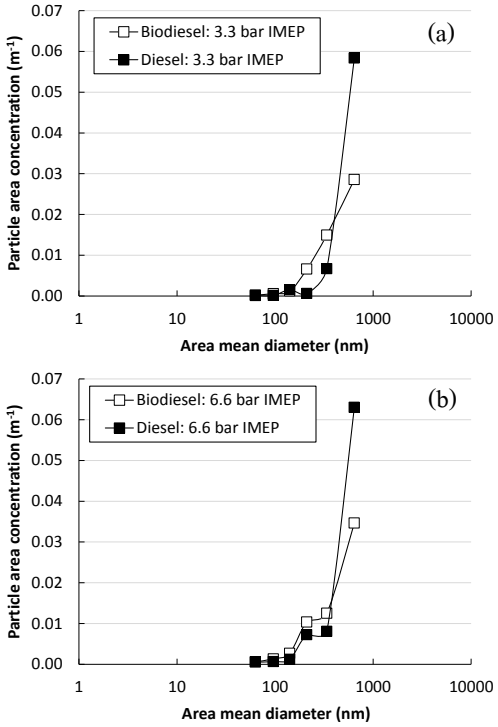

Fig. 10 Particle area size distribution for the engine at (a) 3.3 bar IMEP and (b) 6.6 bar IMEP loads

Fig. 10 shows the distribution of particle surface area concentration over the range of area mean diameter (AMD) from biodiesel and diesel combustions at 3.3 and 6.6 bar IMEP loads, 1,700 rpm. In general, regardless fuel type used, the distributions are left-screwed in the log-scale of AMD range. In the small to medium AMD, biodiesel particles show to be a greater concentration at both loads while the diesel particles show in greater concentration in the large AMD, particularly at the higher load. These trends of the distributions follow the calculation schemes for the surface area concentration (Eq. 8) and the AMD (Eq. 14) that depend on the corresponding number concentration and the D_p.

In novel diesel engines, the physio-geometry of the particulate matter emitted from the combustion chamber becomes more important as it can affect to the exhaust gas after-treatment devices. Therefore, the surface area of the particles will play a vital role as it is a site for catalytic combustion to be taken place. In addition, the data from the previous section have been found that the count mean diameter for both fuels were in the ranges of approximately 280 to 590 nm, and thus accumulation mode. Therefore, the data over the size range of 50 to 1,000 nm will be shown in the following sections.

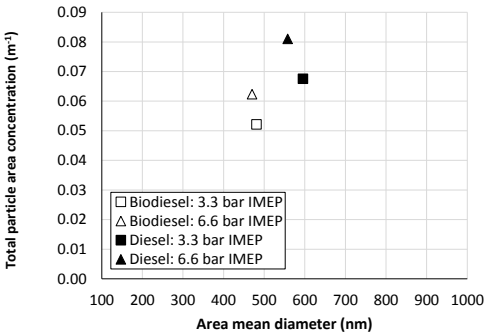

Fig. 11 Relationship between total particle area and area mean diameter

Fig. 11 shows the plot of the total particle area calculated using Eq. (11) and the corresponding AMD. The total particle areas have shown to be higher for diesel fuel at larger size for the two load conditions tested. The total particle areas for biodiesel and diesel fuels were in the ranges of 0.0521 to 0.0623 m^{-1} and 0.0675 to 0.0809 m^{-1}, respectively. The area mean diameter for biodiesel and diesel fuels were in the ranges of 470 to 480 nm and 558 to 596 nm, respectively. Furthermore, the engine running on the higher load generated higher amount of total particle area at smaller size. The reason is due to the calculation schemes for the total surface area (Eq. 11) and the AMD (Eq. 14) that rely on the corresponding number concentration and the D_p.

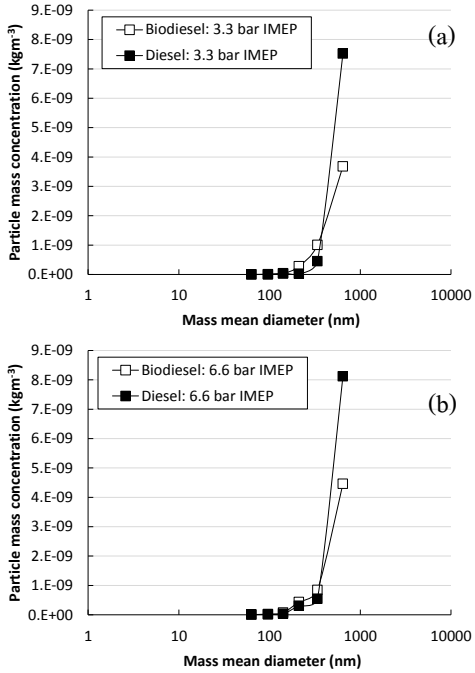

Fig. 12 Particle mass size distribution for the engine at (a) 3.3 bar IMEP and (b) 6.6 bar IMEP loads

Fig. 12 shows the distribution of particle mass concentration over the range of mass mean diameter (MMD) from biodiesel and diesel combustions at 3.3 and 6.6 bar IMEP loads, 1,700 rpm. In general, resemble to the surface area, the distributions are left-screwed in the log-scale of MMD range. As a consequence of particle area, in the small to medium MMD, biodiesel particles show to be a greater

concentration at both loads while the diesel particles show in greater concentration in the large MMD, particularly at the higher load. These trends of the distributions relate to the calculation schemes for the mass concentration (Eq. 9) and the MMD (Eq. 15) that depend on the corresponding number concentration and the D_p.

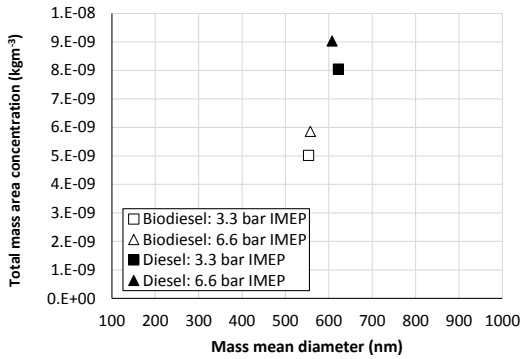

Fig. 13 Relationship between total particle mass and mass mean diameter

Fig. 13 shows the plot of the total particle mass calculated using Eq. (12) and the corresponding MMD. The total particle masses have shown to be higher for diesel fuel at larger size for the two load conditions tested. The total particle mass for biodiesel and diesel fuels were in the ranges of 5.0×10^{-9} to 5.9×10^{-9} kg·m^{-3} and 8.0×10^{-9} to 9.0×10^{-9} kg·m^{-3}, respectively. These total particle masses are in-line with the smoke opacity presented in Fig. 7 [37]. The mass mean diameters for biodiesel and diesel fuels were in the ranges of 553 to 557 nm and 607 to 622 nm, respectively. Furthermore, the engine running on the higher load generated higher amount of total particle mass with comparable size.

4. Conclusion

The experimental investigation on characterizing nano-particle emissions in terms of physio-geometry using palm-based biodiesel in a single-cylinder agricultural engine has revealed the conclusion as the followings.

1. The use of biodiesel in the engine resulted in greater premixed combustion for both engine loads at 3.6 and 6.6 bar IMEP, 1,700 rpm with the start of combustion advanced to the earlier crank angle than that of the diesel fuel, and thus shorter combustion duration.

2. Biodiesel with lower heating value consumed more fuel than that diesel fuel at the same load whereas the engine brake thermal efficiency slightly decreased by 6% and 12% at 3.3 and 6.6 bar IMEP, respectively.

3. For particle number, the distributions for biodiesel are tri-modal log-normal in the CMD range with greater concentration in the nucleation and accumulation modes. The total particle numbers have shown to be higher for biodiesel at smaller size.

4. The distributions of the particle surface area and mass are left-screwed in the log-scale of AMD and MMD ranges, respectively. This leads to the lesser total particle areas and masses for biodiesel fuel at smaller size.

5. Biodiesel combustion resulted in the lower level of smoke opacity than diesel fuel combustion due to inherit oxygenated fuel with near zero sulfur content. The smoke opacity is in agreement with the PM mass calculated based on particle number.

5. Acknowledgment

The authors would like to acknowledge Kasetsart University through Kasetsart University Research and Development Institute for the research funding (Grant Number: V-P(D)42.60).

6. Reference

[1] M.A. Fayad, A. Tsolakis, D. Fernández-Rodríguez, J.M. Herreros, F.J. Martos and M. Lapuerta, "Manipulating Modern Diesel Engine Particulate Emission Characteristics through Butanol Fuel Blending and Fuel Injection Strategies for Efficient Diesel Oxidation Catalysts", Applied Energy 190, 2017, pp. 490-500.

[2] R. Nyström, I. Sadiktsis, T.M. Ahmed, R. Westerholm, J.H. Koegler, A. Blomberg, T. Sandström and C. Boman, "Physical and Chemical Properties of RME Biodiesel Exhaust Particles without Engine Modifications", Fuel 186, 2016, pp. 261–269.

[3] A.K. Agarwal, A. Shrivastava and R.K. Prasad, "Evaluation of Toxic Potential of Particulates Emitted from Jatropha Biodiesel Fuelled Engine", Renewable Energy 99, 2016, pp. 564-572.

[4] W. Sittiwong, W. Seehanam and K. Pianthong, "Effect of Test Chamber Temperature on High Speed Jatropha Oil Blends with Diesel Fuel Behaviors", The Journal of Industrial Technology, 11(3), 2015, pp. 11-26.

[5] C. Poompipatpong, P. Triwong and C. Sikhom, "A Performance Investigation of Small Fishery Boat's Engines Fuelled with Biodiesel B20 for 500-hour Operation", The Journal of Industrial Technology 11(1), 2015, pp. 1-12.

[6] L. Wei, C.S. Cheung and Z. Ning, "Influence of Waste Cooking Oil Biodiesel on Combustion, Unregulated Gaseous Emissions and Particulate Emissions of a Direct-Injection Diesel Engine", Energy 127, 2017, pp. 175-185.

[7] L. Zhu, Y. Xiao, C.S. Cheung, C. Guan and Z. Huang, "Combustion, Gaseous and Particulate Emission of a Diesel Engine Fueled with N-Pentanol (C5 Alcohol) Blended with Waste Cooking Oil Biodiesel", Applied Thermal Engineering 102, 2016, pp. 73–79.

[8] L. Qu, Z. Wang and J. Zhang, "Influence of Waste Cooking Oil Biodiesel on Oxidation Reactivity and Nanostructure of Particulate Matter from Diesel Engine", Fuel 181, 2016, pp. 389–395.

[9] A.V. Bueno, M.P.B. Pereira, J.V. de Oliveira Pontes, F.M.T. de Luna and C.L. Cavalcante Jr., "Performance and Emissions Characteristics of Castor Oil Biodiesel Fuel Blends", Applied Thermal Engineering 125, 2017, pp. 559–566.

[10] D.D. Dutcher, J. Pagels, A. Bika, L. Franklin, M. Stolzenburg, S. Thompson, J. Medrano, N. Brown, D.S. Gross, D. Kittelson and P.H. McMurry, "Emissions from Soy Biodiesel Blends: A Single Particle Perspective", Atmospheric Environment 45, 2011, pp. 3406-3413.

[11] A. Dhar and A.K. Agarwal, “Effect of Karanja Biodiesel Blends on Particulate Emissions from a Transportation Engine”, Fuel 141, 2015, pp. 154–163.

[12] M. Lapuerta, O. Armas, J.J. Hernández and A. Tsolakis, “Potential for Reducing Emissions in a Diesel Engine by Fuelling with Conventional Biodiesel and Fischer–Tropsch Diesel”, Fuel 89, 2010, pp. 3106–3113.

[13] S.S. Gill, A. Tsolakis, J.M. Herreros and A.P.E. York, “Diesel Emissions Improvements through the Use of Biodiesel or Oxygenated Blending Components”, Fuel 95, 2012, pp. 578–586.

[14] J. Su, H. Zhu and S.V. Bohac, “Particulate Matter Emission Comparison from Conventional and Premixed Low Temperature Combustion with Diesel, Biodiesel and Biodiesel–Ethanol Fuels”, Fuel 113, 2013, pp. 221–227.

[15] K. Yang, L. Wei, C.S. Cheung, C. Tang and Z. Huang, “The Effect of Pentanol Addition on the Particulate Emission Characteristics of a Biodiesel Operated Diesel Engine”, Fuel 209, 2017, pp. 132–140.

[16] F. Hedayat, S. Stevanovic, A. Milic, B. Miljevic, M.N. Nabi, A. Zare, S.E. Bottle, R.J. Brown and Z.D. Ristovski, “Influence of Oxygen Content of the Certain Types of Biodiesels on Particulate Oxidative Potential”, Science of the Total Environment 545–546, 2016, pp. 381–388.

[17] P.C. Shukla, T. Gupta, N.K. Labhasetwar, R. Khobaragade, N.K. Gupta and A.K. Agarwal, “Effectiveness of Non-Noble Metal Based Diesel Oxidation Catalysts on Particle Number Emissions from Diesel and Biodiesel Exhaust”, Science of the Total Environment 574, 2017, pp. 1512–1520.

[18] G. Karavalakis, N. Gysel, D.A. Schmitz, A.K. Cho, C. Sioutas, J.J. Schauer, D.R. Cocker and T.D. Durbina, “Impact of Biodiesel on Regulated and Unregulated Emissions, and Redox and Proinflammatory Properties of PM Emitted from Heavy-Duty Vehicles”, Science of the Total Environment 584–585, 2017, pp. 1230–1238.

[19] N. Martin, M. Lombard, K.R. Jensen, P. Kelley, T. Pratt and N. Traviss, “Effect of Biodiesel Fuel on “Real-World”, Nonroad Heavy Duty Diesel Engine Particulate Matter Emissions, Composition and Cytotoxicity”, Science of the Total Environment 586, 2017, pp. 409–418.

[20] X. Wang, Y. Ge, L. Yu and X. Feng, “Comparison of Combustion Characteristics and Brake Thermal Efficiency of a Heavy-Duty Diesel Engine Fueled with Diesel and Biodiesel at High Altitude”, Fuel 107, 2013, pp. 852-858.

[21] H. Tse, C.W. Leung and C.S. Cheung, “Investigation on the Combustion Characteristics and Particulate Emissions from a Diesel Engine Fueled with Diesel-Biodiesel-Ethanol Blends”, Energy 83, 2015, pp. 343-350.

[22] D.B. Kittelson, "Engines and Nanoparticles: A Review", Journal of Aerosol Science 29, 1998, pp. 575-588.

[23] Y. Jung, J. Hwang and C. Bae, "Assessment of Particulate Matter in Exhaust Gas for Biodiesel and Diesel under Conventional and Low Temperature Combustion in a Compression Ignition Engine", Fuel 165, 2016, pp. 413–424.

[24] S. Thitipatanapong, S. Chuepeng and P. Visuwan, "Characterization of Particulate from Biodiesel-Blended Engine Equipped with Exhaust Nonthermal Plasma Charger Using Thermo-Gravimetric Analysis", The 11th International Conference on Automotive Engineering, Bangkok, Thailand, 2015.

[25] M.M. Rahman, A.M. Pourkhesalian, M.I. Jahirul, S. Stevanovic, P.X. Pham, H. Wanga, A.R. Masri, R.J. Brown and Z.D. Ristovski, "Particle Emissions from Biodiesels with Different Physical Properties and Chemical Composition", Fuel 134, 2014, pp. 201–208.

[26] S. Pinzi, P. Rounce, J.M. Herreros, A. Tsolakis and M.P. Dorado, "The Effect of Biodiesel Fatty Acid Composition on Combustion and Diesel Engine Exhaust Emissions", Fuel 104, 2013, pp. 170–182.

[27] P. Rounce, A. Tsolakis and A.P.E. York, "Speciation of Particulate Matter and Hydrocarbon Emissions from Biodiesel Combustion and Its Reduction by Aftertreatment", Fuel 96, 2012, pp. 90–99.

[28] N. Savic, M.M. Rahman, B. Miljevic, H. Saathoff, K.H. Naumann, T. Leisner, J. Riches, B. Gupta, N. Motta and Z.D. Ristovski, "Influence of Biodiesel Fuel Composition on the Morphology and Microstructure of Particles Emitted from Diesel Engines", Carbon 104, 2016, pp. 179-189.

[29] M. Salamanca, F. Mondragón, J.R. Agudelo and A. Santamaría, "Influence of Palm Oil Biodiesel on the Chemical and Morphological Characteristics of Particulate Matter Emitted by a Diesel Engine", Atmospheric Environment 62, 2012, pp. 220-227.

[30] D. Buono, A. Senatore and M.V. Prati, "Particulate Filter Behaviour of a Diesel Engine Fueled with Biodiesel", Applied Thermal Engineering 49, 2012, pp. 147-153.

[31] P. Intra and N. Tippayawong, "Development of a Fast-Response, High-Resolution Electrical Mobility Spectrometer", Korean Journal of Chemical Engineering 28(1), 2011, pp. 279-286.

[32] J.B. Heywood, *"Internal Combustion Engine Fundamentals"*, McGraw-Hill, 1988.

[33] S. Chuepeng, A. Tsolakis, K. Theinnoi, H.M. Xu, M.L. Wyszynski and J. Qiao, "A Study of Quantitative Impact on Emissions of High Proportion RME-Based Biodiesel Blends", SAE 2007 Fuels and Emissions Conference, Cape Town, South Africa, 2007.

[34] S. Chuepeng, H.M. Xu, A. Tsolakis, M.L. Wyszynski, P. Price, R. Stone, J. C. Hartland and J. Qiao, "Particulate Emissions from a Common Rail Fuel Injection Diesel Engine with RME-based Biodiesel Blended Fuelling Using Thermo-Gravimetric Analysis", SAE 2008 World Congress, Detroit, U.S.A., 2008.

[35] S. Chuepeng, K. Theinnoi, A. Tsolakis, H.M. Xu, M.L. Wyszynski, A.P.E. York, J.C. Hartland and J. Qiao, "Investigation into Particulate Size Distributions in the Exhaust Gas of Diesel Engines Fuelled with Biodiesel Blends", Journal of KONES Powertrain and Transport 15(3), 2008, pp. 75-82.

[36] S. Chuepeng, H.M. Xu, A. Tsolakis, M.L. Wyszynski and J.C. Hartland, "Nano-particle Number from Biodiesel Blends Combustion in a Common Rail Fuel Injection System Diesel Engine Equipped with Exhaust Gas Recirculation", Combustion Engines 138(3), pp. 28-36.

[37] S. Chuepeng, H.M. Xu, A. Tsolakis, M. Wyszynski and P. Price, "Particulate Matter Size Distribution in the Exhaust Gas of a Modern Diesel Engine Fuelled with a Biodiesel Blend", Biomass and Bioenergy 35, 2011, pp. 4280-4289.